Front. Optoelectron. 2017, 10(2): 124–131
DOI 10.1007/s12200-017-0682-z

RESEARCH ARTICLE

Broadband and conformal metamaterial absorber

Xiangkun KONG (✉)[1,2], Junyi XU[1], Jin-jun MO[3], Shaobin LIU[1]

1 Key Laboratory of Radar Imaging and Microwave Photonics, Ministry of Education, College of Electronic and Information Engineering, Nanjing University of Aeronautics and Astronautics, Nanjing 210016, China
2 State Key Laboratory of Millimeter Waves, Southeast University, Nanjing 210096, China
3 College of Electronic Science and Engineering, National University of Defense Technology, Changsha 410073, China

Abstract In this study, a new broadband and conformal metamaterial absorber using two flexible substrates was proposed. Simulation results showed that the proposed absorber exhibited an absorption band from 6.08 to 13.04 GHz and a high absorption of 90%, because it was planar. The absorber was broadband as its relative absorption bandwidth was 72.8%. Moreover, the proposed absorber was insensitive to the polarization of the TE and TM waves. The absorber was ultra-thin; its total thickness was only 0.07λ at the lowest operating frequency. Furthermore, different regions of absorption can be adjusted by lumping and loading two resistors onto the polyimide film, respectively. Moreover, compared with the conventional microwave absorber, the absorption bandwidth of the proposed absorber can be broadened and enhanced when it was bent and conformed to the surface of objects. Experimental and simulation results were in agreement. The proposed absorber is a promising absorbing element in scientific and technical applications because of its broadband absorption, polarization insensitivity, and flexible substrates.

Keywords absorber, metamaterials, flexible, broadband, conformal

1 Introduction

Electromagnetic (EM) metamaterials [1,2] are arrays of structured sub-wavelength elements that may be described as effective materials due to their electric permittivity ($\varepsilon(\omega)$) and magnetic permeability ($\mu(\omega)$). Metamaterials can achieve a negative refractive index, which is a phenomenon first postulated by Veselago (1968) [3]. In addition to having a negative refractive index, metamaterials have many exotic applications, including invisibility cloaking [4], concentrators [5], perfect lenses [6,7], hyperlens [8], and aberration free lenses [9]. Since Landy et al. (2008) proposed a metamaterial absorber (MMA) composed of electric resonators and cut wires [10], the use of artificial EM metamaterials in absorbers has attracted considerable interest because of the nearly perfect absorption of these materials. Up to the present, numerous efforts and studies have been devoted to this area with the goal of designing absorbers with excellent performances in multiband [11–15], broadband [16–20], and other modes of operation [21–24]. However, most of the existing absorbers reported in the literature were made of FR-4, which cannot be bent.

Therefore, a flexible absorber has become a research interest in recent years. Singh et al. proposed single- and dual-band 77/95/110 GHz MMAs on a flexible polyimide (PI) substrate [25]. Yoo et al. researched a flexible and elastic low-frequency MMA [26]. A free-standing highly flexible metamaterial operating in the terahertz frequency range was proposed by Tao et al. [27]. Kim et al. researched a flexible inkjet-printed MMA on paper [28]. Their substrates were flexible; thus, these absorbers can be applied to the surface of irregular object, and they can satisfactorily absorb incident waves. However, flexible absorbers were mostly designed to operate at a single frequency or multi-frequencies due to the limitation of thickness; as a result, the bandwidth is difficult to expand. Several studies have reported on broadband and ultra-thin MMAs. For example, the design in Ref. [29] achieved a bandwidth of approximately 112% and a thickness of 0.04λ, where λ is the wavelength at the lowest operating frequency. In Ref. [30], a double-square-loop array design was adopted to obtain a fractional bandwidth of 128.2% with a thickness of 0.088λ. Four resistively loaded hexagonal loop elements were used to realize a bandwidth of 108% at normal incidence with a thickness of 0.078λ [31]. However, none of these MMAs used a flexible substrate to attach to irregularly shaped surfaces.

Received December 6, 2016; accepted March 9, 2017

E-mail: xkkong@nuaa.edu.cn

In this study, we present a conformal, broadband, polarization-insensitive, and ultra-thin microwave absorber that utilizes a resonant structure to provide good impedance match to the air. In view of the extensive application of the X-band (8–12 GHz) and C-band (4–8 GHz) to radars, the proposed absorber is designed to absorb 90% of normal incident microwaves from 6.08 to 13.04 GHz, which covers the entire X-band and half of the C-band. The absorber is ultra-thin with a total thickness of only 0.07λ at the lowest operating frequency. High absorption can still be achieved as the angle of incidence increases from 0° to 60°.

The fabrication and measurement processes have been presented in our previous paper [14]. According to the measurement results, the relative absorption bandwidth of the sample can be broadened and enhanced to 100% when the sample is coated on a cylinder. The proposed structure can be used as a conformal, broadband, thin, wide-incident-angle, and polarization-insensitive microwave absorber in target stealth, EM shielding, and cloaking because of its flexible substrate and high absorption characteristics.

2 Design and theory

The complete microwave absorber is the periodic extension of the unit cell in both x- and y-directions. The front and side views of the absorber are shown in Figs. 1(a) and 1(b). In each unit cell, the proposed absorber was fabricated using a PI film, whose thickness and relative permittivity are respectively denoted by t_1 and ε_1. A PI film with loss tangent $\tan\delta = 0.006$ is often used as the dielectric substrate of a flexible printed circuit because it is pliable [32].The resonator consisted of three nested cross-square rings to induce ohmic loss and effectively dissipate the coupled EM energy to heat. The resonator was patterned on the PI film, as shown in Fig. 1(c). The nested cross-square rings structure possessed three resonances resulting from the centrally symmetric cross-square ring structure, as well as the coupling between neighboring cross-square ring structures. The polarization-insensitive property was also attributable to the centrally symmetric cross-square ring structure. In addition, rubber with loss tangent $\tan\delta = 0.03$ was introduced to facilitate the fabrication of the proposed absorber [33]. The thickness and relative permittivity of the rubber are denoted as h_2 and ε_2, respectively. Metal tape was pasted at the back of the flexible rubber layer to fabricate a back-metal plane. In the design, the optimized geometric parameters of the unit cell were as follows: $t_1 = 0.18$ mm, $\varepsilon_1 = 3.5$, $t_2 = 3.5$ mm, $\varepsilon_2 = 3$, $L = 14.4$ mm, $a_1 = 9$ mm, $a_2 = 6.5$ mm, $a_3 = 5$ mm, $b_1 = 5$ mm, $b_2 = 2.6$ mm, $b_3 = 0.2$ mm, $w_1 = 0.2$ mm, $w_2 = 0.5$ mm, $w_3 = 0.8$ mm, $R_1 = 270\ \Omega$, and $R_2 = 150\ \Omega$.

The absorption of the proposed absorber can be calculated by the following equation: $A(\omega) = 1 -$

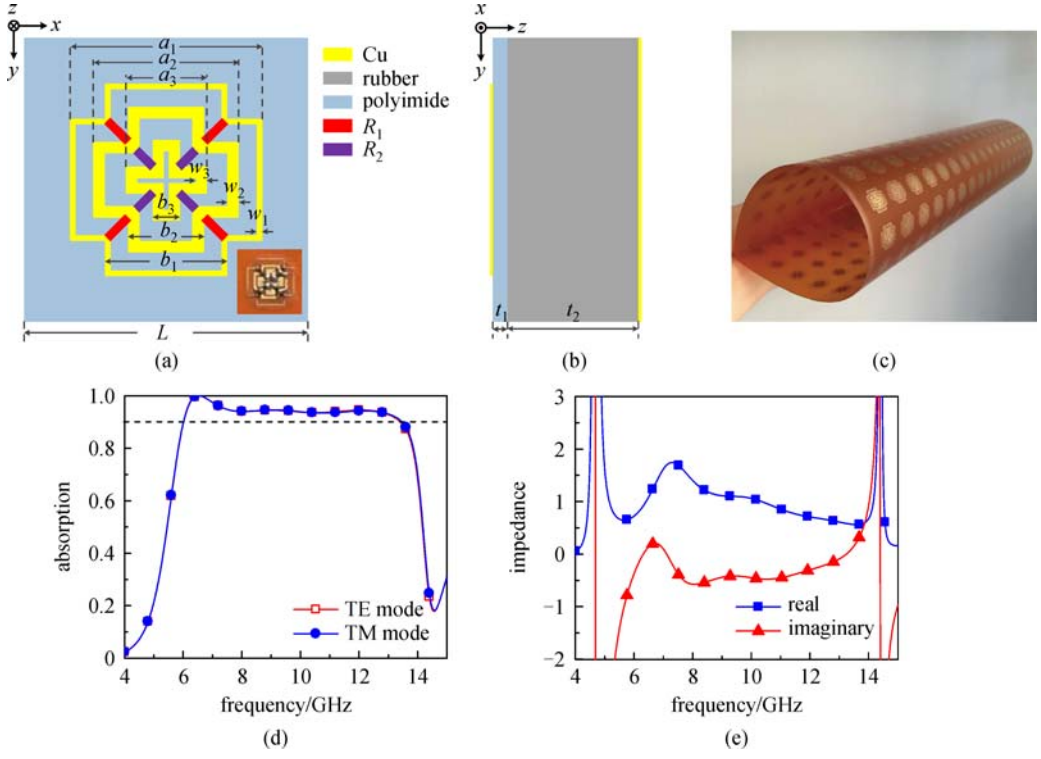

Fig. 1 (a) Top view of the conformal absorber; (b) side view of the conformal absorber; (c) resonator patterned on a PI film; (d) simulated and measured absorption with respect to the frequency; (e) calculated real and imaginary parts of the impedance

$|S_{11}(\omega)|^2-|S_{21}(\omega)|^2$, where $A(\omega)$, $|S_{11}(\omega)|^2$, and $|S_{21}(\omega)|^2$ are the absorption, reflection, and transmission at the angular frequency ω, respectively. The ground plane under the bottom layer prevented the waves to pass through the absorber; thus, the transmission may be considered zero. The simulated absorptions of the proposed absorber for the TE and TM waves are shown in Fig. 1(d). The absorber achieved three resonance frequencies at 6.53, 9.07, and 12.18 GHz. The absorptions exceeded 90% from 6.08 to 13.04 GHz, and the full-width-at-half-maximum [18] absorption bandwidth was 8.63 GHz, which was from 5.51 to 14.14 GHz. The impedance of the absorber was matched to the air to achieve perfect absorption, and the transmitted waves were dissipated due to the ground plane. The total impedance of the structure was obtained from the combination of the impedances of the resonant structure and dielectric layers with the ground plane. The effective impedance of the structure can be obtained using the following equation [34]:

$$Z_{\text{eff}}(\omega)=\sqrt{\frac{\mu_{\text{eff}}(\omega)}{\varepsilon_{\text{eff}}(\omega)}}=\sqrt{\frac{(1+S_{11}(\omega))^2}{(1-S_{11}(\omega))^2}},$$

where $\varepsilon_{\text{eff}}(\omega)$ and $\mu_{\text{eff}}(\omega)$ are the effective permittivity and permeability, respectively. The real and imaginary parts of the impedance are derived from the simulated complex S-parameters. As shown in Fig. 1(e), the calculated real and imaginary parts of the impedance were nearly unity, and the real part of the impedance was nearly unity when the imaginary part of the impedance approached zero in the absorption band. Therefore, impedance matching with air was achieved; as a result, the reflection from the absorber was minimized.

3 Simulation results

A full-wave EM simulation was performed to obtain the reflection parameter S_{11} and transmission parameter S_{21} by using the commercial program CST Microwave Studio 2010. The periodic boundary conditions were applied to the x- and y-directions, and the absorbing boundary conditions were applied to the z-direction. A cross-square ring resonator was used because of its centrally symmetric configuration, which is less sensitive to the polarization of the incident wave. Consequently, the absorption was nearly polarization-insensitive due to the symmetric structure. The simulation results show that the absorption was nearly unchanged for TE and TM polarizations, as shown in in Fig. 1(d). These results demonstrate the insensitivity to polarization of the absorber structure. As shown in Fig. 2, the absorption decreased gradually as the angle of incidence increased for every polarization. Nevertheless, the absorption was still higher than 60% with a wide angle of incidence of up to 60°.

The geometric parameters, as well as resistance, were selected to obtain the desired wave absorptions at three resonance frequencies to design the broadband absorber. These parameters were further optimized to merge the three resonances spectrally and provide broadband characteristics. For example, as the dimension (a_1) of the outer cross-square ring increased, the first absorption frequency, as well as the absorption band, shifted to a lower frequency range, as shown in Fig. 3(a).

In addition, the metallic resonant structure with a high Q factor can be utilized in such applications as narrow-band filters and oscillators that require high selectivity and low loss. The Q factor of the structure should be reduced to achieve broadband absorption. This goal can be achieved by increasing the resistance, which also dissipates energy, thereby minimizing reflection over a broad frequency range. Two groups of lumped resistors were used to construct the resonant structure for increased resistance. Figure 3(b) shows that increasing the resistance of R_1 from 220 to 320 Ω can change the absorption between the first and second frequencies, but such an increase exerted no influence on the third frequency. The advantage of the proposed structure is that it allows for the increase in the absorption between two peak frequencies alone by optimizing the corresponding resistors to enhance the coupling between two cross-square rings. Thus, placing the lumped resistors between two rings renders the

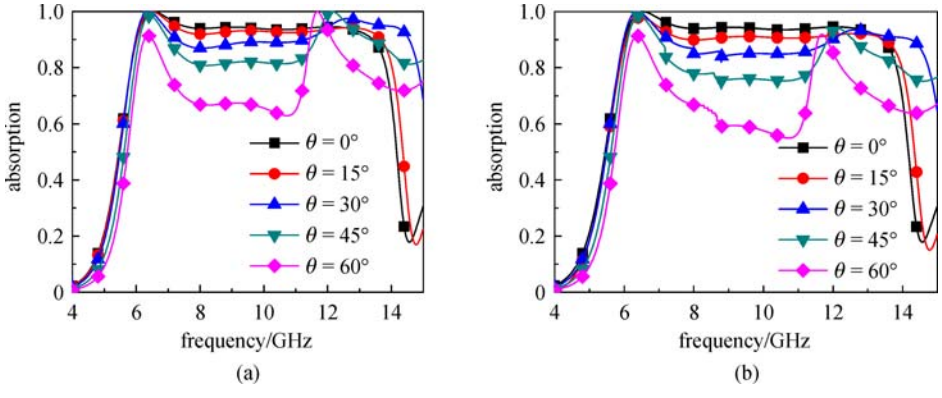

Fig. 2 Simulated absorptions for different angles of incidence for (a) TE and (b) TM polarizations

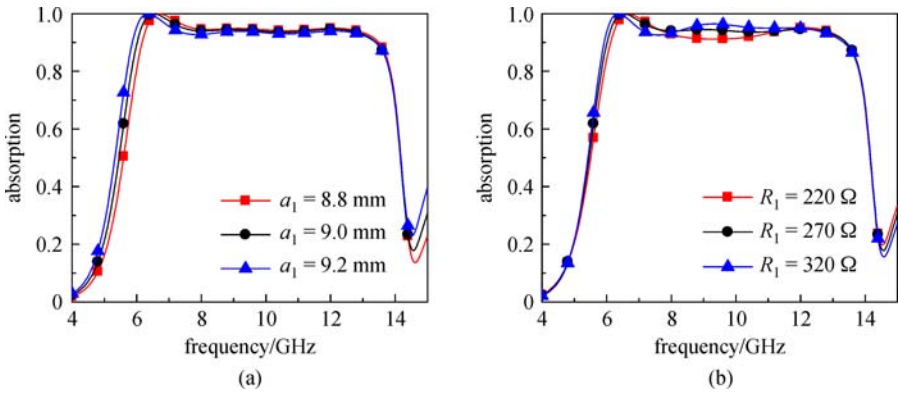

Fig. 3 Simulated absorptions for different values of (a) geometric parameter a_1 and (b) resistor R_1

absorption to be easily tunable. The simulation also showed that geometric parameters a_2, a_3, and R_2 exerted similar influences on the proposed absorber. By merging the three resonances, we achieved a broad bandwidth of 72.8% of the center frequency.

The surface current distribution and electrical field distribution were simulated and analyzed using the CST software to understand the origin of these three absorption peaks. Figures 4(a)–4(c) show the top view of the simulated current distribution on the surface of the absorber structure at the three absorption peak frequencies, whereas Figs. 4(d)–4(f) show that in the central cross section. In these figures, the arrow indicates the direction of flow, and the color represents the intensity.

As shown in Figs. 4(a) and 4(d), the directions of the surface current at the frequency 6.53 GHz on the three cross-square rings (outer, middle, and inner) were antiparallel with that of the surface current on the ground plane, and the current intensity in the outer ring was the strongest. The currents on the two surfaces flowed in opposite directions and constituted a circulating current loop, which was formed on the plane perpendicular to the direction of the incident magnetic field. The magnetic resonance at the frequency of 6.53 GHz was mainly caused by the outer ring. Figures 4(b) and 4(e) show the surface currents at the frequency of 9.07 GHz, where the behavior was similar to that at the frequency of 6.53 GHz. However, only the currents in the middle and inner rings were antiparallel with the direction of the surface current on the ground plane, with the current intensity in the middle ring being stronger. Therefore, the magnetic response was mainly achieved by the middle ring at 9.07 GHz. At the

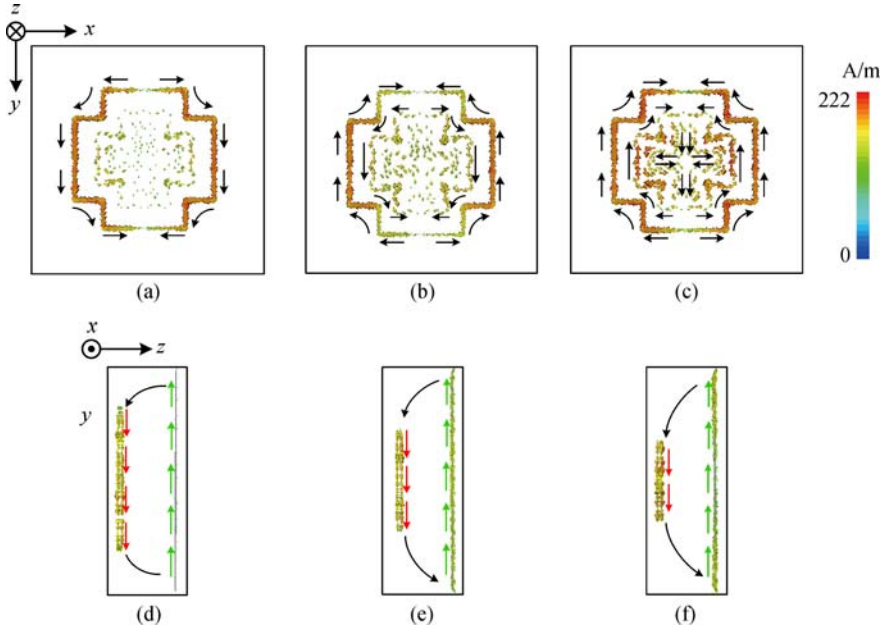

Fig. 4 Simulated current distributions on the surface at the three resonance frequencies: (a)–(c) top view and (d)–(f) central cross section

frequency of 12.18 GHz, antiparallel surface current flowed in the inner ring, as shown in Figs. 4(c) and 4(f), and this current led to the magnetic response. In all cases, the resonant modes at the three frequencies were *LC* resonances, and the energies flowing in the cross-square rings eventually dissipated due to the high ohmic loss of the lumped resistors that were used to form the structure. These results verified that the three absorption peaks were contributed by the fundamental resonance of the cross-square ring structure and the coupling between cross-square ring structures. The merging of the three resonances with overlapping spectra proves the broadband performance of the proposed absorber.

4 Experimental results

A 16 × 16-unit cell sample with an area of 230.4 mm × 230.4 mm was fabricated by first depositing a 62-nm-thick copper layer on a 0.18-mm-thick PI film by sputtering. The cross-square ring structures were then patterned using the standard printed circuit board technology. The PI film with patterned copper structure was then attached to a thicker and more flexible rubber layer. A top view of the fabricated cross-square array on the PI film is shown in Fig. 5(a).

As shown in Fig. 5(b), a pair of broadband horn antennas were used to transmit and receive EM waves. The horn antennas had a voltage standing wave ratio of < 2 and a wide frequency range of 1–18 GHz. The fabricated sample and the horn antennas were placed at the same height but apart at a distance of $> 2L^2/\lambda_0$, where L is the maximum dimension of the horn antenna to minimize the effect of near-field interference and diffraction. An Agilent N5245A vector network analyzer was connected to the two wideband horn antennas to measure the absorber sample.

The reflections at the front and back of the planar absorber were measured. The difference between them was expressed in decibels. Figures 6(a)–6(c) show the measured planar absorptions at different incident angles (θ) of the incident wave. The absorption at normal incidence of the fabricated sample was greater than 90% in the frequency range of 6.11–12.94 GHz, and the bandwidth was 66.4% of the center frequency. With increasing incident angle, the measured absorption in the high-frequency region increased and remained high until the angle of incidence reached 60°. The experimental results show good agreement with the simulations results.

Then, the conformal sample was measured in the same environment. The sample was conformed to the surface of the cylinder with different radii, as shown in Fig. 7(a); thus, the corresponding central angles (α) were likewise different. The central angles (α) varied from 60° to 180°, whereas the normal incident waves are maintained at the center of the sample. Accordingly, the incident angles of the unit cell at both edges are denoted by $\alpha/2$ in Fig. 7(b) and ranged from 30° to 90°.

The measured absorptions at central angles (α) ranging from 60° to 180° are shown in Fig. 8. As the central angle increased, the absorption band of the sample widened and was enhanced. For example, when α was 60°, the absorption band covered the range of 6–13.2 GHz, which is nearly the same as the results of planar measurement. However, when α was 180°, the absorption band covered the range of 5–15 GHz, because the incident angles of the unit cells at different parts of the sample were from 0° to 90° when α was 180°. On the basis of the planar measurement results, the absorption in the high-frequency region would be enhanced when the incident angle (θ) increased. Thus, the total absorption band was broadened when the metamaterials conformed to the cylinder.

5 Conclusion

In this study, a new conformal, broadband, polarization-insensitive, and ultra-thin microwave absorber based on a

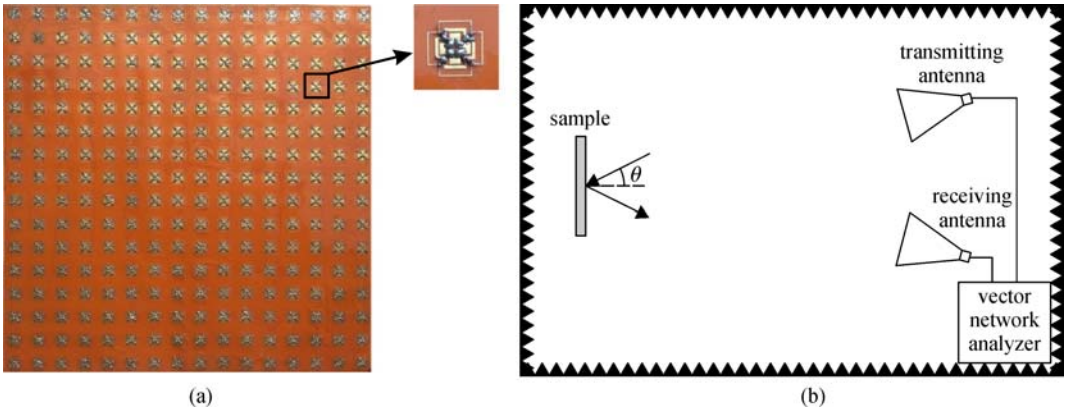

Fig. 5 (a) Photograph of the fabricated measurement sample; (b) planar measurement environment

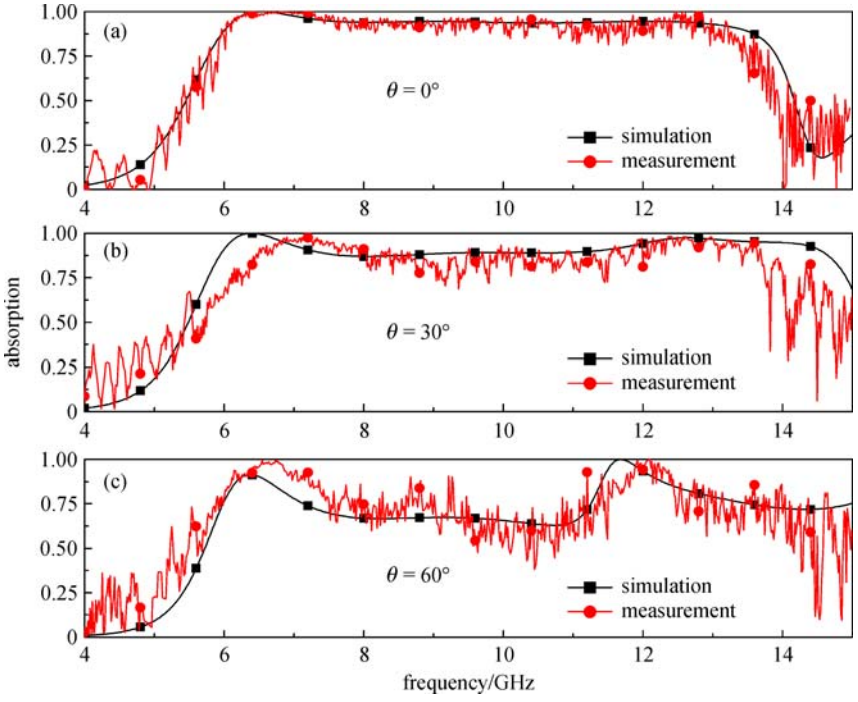

Fig. 6 Measured absorptions at different incident angles (0°– 60°) of the incident wave

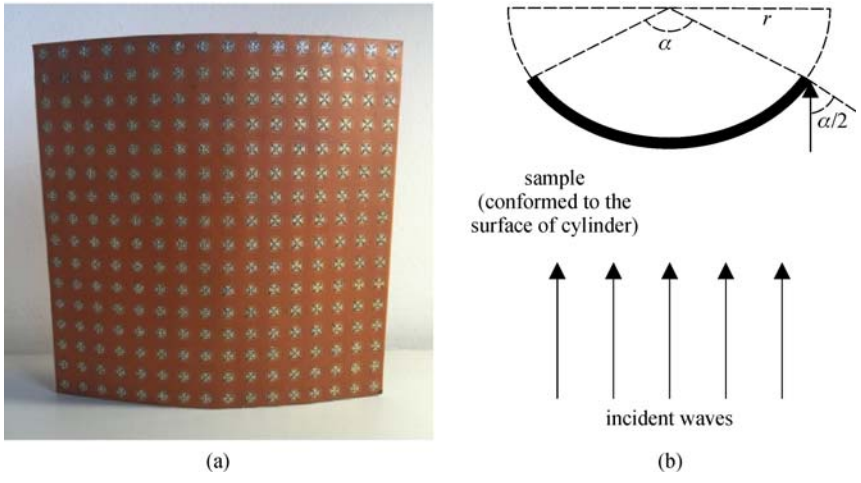

Fig. 7 (a) Sample conformed to the surface of the cylinder; (b) conformal measurement at different central angles (α = 60°–180°)

cross-square array was studied. The proposed planar absorber could absorb incident waves when the angle (θ) was from 0° to 60°. The lumped resistors between the cross-square rings reduced the Q factor of the structure; consequently, the absorption exceeded 90% in the 6.08–13.04 GHz frequency range, and the relative absorption bandwidth was 72.8%. The absorption ranges of the three absorption peak frequencies were independent and tunable. Moreover, the absorption band was broadened and enhanced from 5 to 15 GHz, and it exhibited a relative absorption bandwidth of 100% when the metamaterials conformed to the surface of the cylinder. The centrally symmetric structure rendered the absorber insensitive to the polarization of the incident waves. Furthermore, the total thickness of the absorber was only 0.07λ at the lowest operating frequency. EM field and surface current distribution were analyzed for a better understanding of the mechanism of the high absorption. The simulation and experimental results were in good agreement. In summary, the advantages of the fabricated absorber validate its potential application to target stealth, EM shielding, and cloaking.

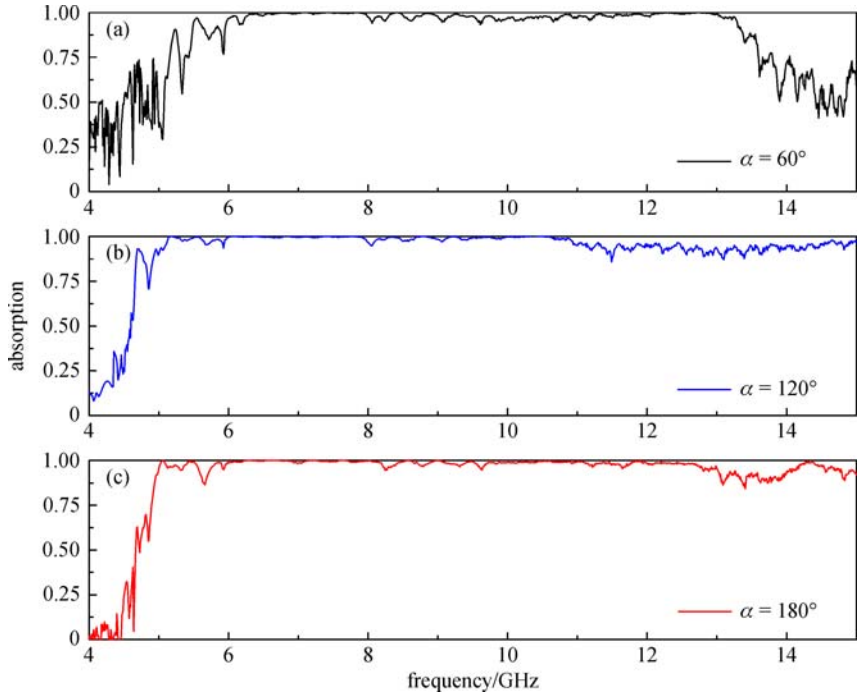

Fig. 8 Measured absorptions at different central angles (α = 60°–180°)

Acknowledgements This work was supported by the Fundamental Research Funds for the Central Universities (No. NJ20160008), the National Natural Science Foundation of China (Grant No. 61471368), the Natural Science Foundation of Jiangsu Province of China (No. BK20150757), the Open Research Program in China's State Key Laboratory of Millimeter Waves (No. K201609), the China Postdoctoral Science Foundation (No. 2016M601802), and the Jiangsu Planned Projects for Postdoctoral Research Funds (No. 1601009B).

References

1. Pendry J B, Holden A J, Stewart W J, Youngs I. Extremely low frequency plasmons in metallic mesostructures. Physical Review Letters, 1996, 76(25): 4773–4776
2. Pendry J B, Holden A J, Robbins D J, Stewart W J. Magnetism from conductors and enhanced nonlinear phenomena. IEEE Transactions on Microwave Theory and Techniques, 1999, 47(11): 2075–2084
3. Veselago V G. The electrodynamics of substances with simultaneously negative values of ε and μ. Soviet Physics-Uspekhi, 1968, 10(4): 509–514
4. Schurig D, Mock J J, Justice B J, Cummer S A, Pendry J B, Starr A F, Smith D R. Metamaterial electromagnetic cloak at microwave frequencies. Science, 2006, 314(5801): 977–980
5. Bian B, Liu S, Wang S, Kong X, Guo Y, Zhao X, Ma B, Chen C. Cylindrical optimized nonmagnetic concentrator with minimized scattering. Optics Express, 2013, 21(S2): A231–A240
6. Pendry J B. Negative refraction makes a perfect lens. Physical Review Letters, 2000, 85(18): 3966–3969
7. Fang N, Lee H, Sun C, Zhang X. Sub-diffraction-limited optical imaging with a silver superlens. Science, 2005, 308(5721): 534–537
8. Liu Z, Lee H, Xiong Y, Sun C, Zhang X. Far-field optical hyperlens magnifying sub-diffraction-limited objects. Science, 2007, 315 (5819): 1686
9. Schurig D, Smith D R. Negative index lens aberrations. Physical Review E: Statistical, Nonlinear, and Soft Matter Physics, 2004, 70 (6): 065601
10. Landy N I, Sajuyigbe S, Mock J J, Smith D R, Padilla W J. Perfect metamaterial absorber. Physical Review Letters, 2008, 100(20): 207402
11. Shen X, Yang Y, Zang Y, Gu J, Han J, Zhang W, Jun Cui T. Triple-band terahertz metamaterial absorber: design, experiment, and physical interpretation. Applied Physics Letters, 2012, 101(15): 154102
12. Xu H, Wang G, Qi M, Liang J, Gong J, Xu Z. Triple-band polarization-insensitive wide-angle ultra-miniature metamaterial transmission line absorber. Physical Review B: Condensed Matter and Materials Physics, 2012, 86(20): 205104
13. Mao Z, Liu S, Bian B, Wang B, Ma B, Chen L, Xu J. Multi-band polarization-insensitive metamaterial absorber based on Chinese ancient coin-shaped structures. Journal of Applied Physics, 2014, 115(20): 204505
14. Bian B, Liu S, Wang S, Kong X, Zhang H, Ma B, Yang H. Novel triple-band polarization-insensitive wide-angle ultra-thin microwave metamaterial absorber. Journal of Applied Physics, 2013, 114(19): 194511
15. Ye Q, Liu Y, Lin H, Li M, Yang H. Multi-band metamaterial absorber made of multi-gap SRRs structure. Applied Physics A, Materials Science & Processing, 2012, 107(1): 155–160
16. Liu Y, Gu S, Luo C, Zhao X. Ultra-thin broadband metamaterial absorber. Applied Physics A, Materials Science & Processing , 2012, 108(1): 19–24
17. Yang G, Liu X, Lv Y, Fu J, Wu Q, Gu X. Broadband polarization-

insensitive absorber based on gradient structure metamaterial. Journal of Applied Physics, 2014, 115(17): 17E523
18. Wang B, Liu S, Bian B, Mao Z, Liu X, Ma B, Chen L. A novel ultrathin and broadband microwave metamaterial absorber. Journal of Applied Physics, 2014, 116(9): 094504
19. Pang Y, Cheng H, Zhou Y, Li Z, Wang J. Ultrathin and broadband high impedance surface absorbers based on metamaterial substrates. Optics Express, 2012, 20(11): 12515–12520
20. Sun L, Cheng H, Zhou Y, Wang J. Broadband metamaterial absorber based on coupling resistive frequency selective surface. Optics Express, 2012, 20(4): 4675–4680
21. Wu C, Neuner Iii B, John J, Milder A, Zollars B, Savoy S. Large-area, wide-angle, spectrally selective plasmonic absorber. Physical Review B: Condensed Matter and Materials Physics, 2011, 84(7): 173 – 177
22. Zhu B, Wang Z, Huang C, Feng Y, Zhao J, Jiang T. Polarization insensitive metamaterial absorber with wide incident angle. Progress in Electromagnetics Research, 2010, 101: 231–239
23. Li L, Yang Y, Liang C. A wide-angle polarization-insensitive ultra-thin metamaterial absorber with three resonant modes. Journal of Applied Physics, 2011, 110(6): 063702
24. Bhattacharyya S, Ghosh S, Srivastava K V. Triple band polarization-independent metamaterial absorber with bandwidth enhancement at X-band. Journal of Applied Physics, 2013, 114(9): 094514
25. Singh P K, Korolev K A, Afsar M N, Sonkusale S. Single and dual band 77/95/110 GHz metamaterial absorbers on flexible polyimide substrate. Applied Physics Letters, 2011, 99(26): 264101
26. Yoo Y J, Zheng H Y, Kim Y J, Rhee J Y, Kang J H, Kim K W, Cheong H, Kim Y H, Lee Y P. Flexible and elastic metamaterial absorber for low frequency, based on small-size unit cell. Applied Physics Letters, 2014, 105(4): 041902
27. Tao H, Strikwerda A C, Fan K, Bingham C M, Padilla W J, Zhang X, Averitt R D. Terahertz metamaterials on free-standing highly-flexible polyimide substrates. Journal of Physics D: Applied Physics, 2008, 41(23): 232004
28. Kim H K, Ling K, Kim K, Lim S. Flexible inkjet-printed metamaterial absorber for coating a cylindrical object. Optics Express, 2015, 23(5): 5898–5906
29. Clavijo S, Diaz R E, McKinzie W E. Design methodology for sievenpiper high-impedance surfaces: an artificial magnetic conductor for positive gain electrically small antennas. IEEE Transactions on Antennas and Propagation, 2003, 51(10): 2678–2690
30. Shang Y, Shen Z, Xiao S. On the design of single-layer circuit analog absorber using double-square-loop array. IEEE Transactions on Antennas and Propagation, 2013, 61(12): 6022–6029
31. Zabri S N, Cahill R, Schuchinsky A. Compact FSS absorber design using resistively loaded quadruple hexagonal loops for bandwidth enhancement. Electronics Letters, 2015, 51(2): 162–164
32. Ponchak G E, Downey A N. Characterization of thin film microstrip lines on polyimide. IEEE Transactions on Components, Packaging, and Manufacturing Technology, Part B, 1998, 21(2): 171–176
33. Schallamach A, Thirion P. Dielectric loss in swollen rubber. Transactions of the Faraday Society, 1949, 45: 605–611
34. Jang T, Youn H, Shin Y J, Guo L J. Transparent and flexible polarization-independent microwave broadband absorber. ACS Photonics, 2014, 1(3): 279–284

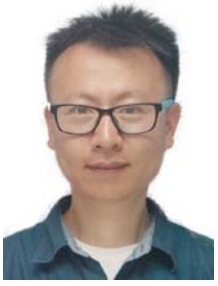

Xiangkun Kong received the Ph.D. degree in communication and information systems from the Nanjing University of Aeronautics and Astronautics (NUAA) in 2015. He has been an associate professor in NUAA since his promotion in July 2015. Currently, he is working at the University of St. Andrews in the UK as an academic visitor supported by China Scholarship Council. His main research interests include the plasma stealth, plasma photonic crystal, electromagnetic properties of metamaterials, and computational electromagnetics. He has published more than 60 papers in different academic journals, including *Applied Physics Letters*, *Optics Express*,and *IEEE Journal of Selected Topics in Quantum Electronics*, and has been cited 1099 times.

Junyi Xu received the M.S. degree from the College of Electronic and Information Engineering of the Nanjing University of Aeronautics and Astronautics in 2015. She is currently working as an engineer in NARI Technology Development Co. at Nanjing. She specializes in flexible metamaterial devices.

Jinjun Mo received the B.Eng., M.Eng., and Ph.D. degrees from the National University of Defense Technology (NUDT), China in 1997, 2000, and 2004, respectively, all in electronic engineering. He was a visiting researcher in the University of Montreal, Canada from 2011 to 2012. He is currently an associate professor at the College of Electronic Science and Engineering of the NUDT. His research interests include scattering problems, computational electromagnetics, and plasma application.

Shaobin Liu received the Ph.D. degree in electronics science and technology from the National University of Defense Technology in 2004. However, in 2003, he was already promoted as professor. He is currently a professor of electromagnetic and microwave technology at the Nanjing University of Aeronautics and Astronautics. His research focuses on plasma stealthy antennas, microwave, radio frequency, electromagnetic compatibility.